Comparative **UV-Visible and Photoluminescence,** analysis of PVA/TiO_2, PVA/ZrO_2 and PVA/TiO_2/ZrO_2 Composites

[1] Dr Jyotsna Chauhan,[2]akansha mehto, [3]Shaswat Chauhan

[1]Professor in RGPV, [2]Research scholar,[3] BITS Pilani GOA (electrical)

Abstract: To synthesize and characterize uniform and stable PVA-based composite membranes incorporating TiO_2 and ZrO_2 nanoparticles (PVA/TiO_2, PVA/ZrO_2, and PVA/TiO_2/ZrO_2) using the solution casting method. And investigate the structural, morphological, surface chemistry and optical properties of these composite membranes through advanced characterization techniques encompassed X-ray diffraction (XRD) study, UV-visible absorption spectroscopy, photoluminescence (PL) spectroscopy, transmission electron microscopy (TEM), Fourier-transform infrared (FTIR) spectroscopy, and atomic force microscopy (AFM) analysis and develop hybrid membranes that exhibit more improved characteristics because of composites versatile properties resulting from the combining of two inorganic structural components with polymer. These characteristics offer an appealing choice for a range of applications.

[Dr Jyotsna Chauhan, akansha mehto, Shaswat Chauhan. Comparative **UV-Visible and Photoluminescence,** analysis of PVA/TiO_2, PVA/ZrO_2 and PVA/TiO_2/ZrO_2 Composites. *N Y Sci J* 2026;19(8):35-49]. ISSN 1554-0200 (print); ISSN 2375-723X (online). http://www.sciencepub.net/newyork. 04. Doi: 10.7537/marsnys190826.04

Keywords: photoluminescence (PL) spectroscopy; nanoparticles; XRD

Introduction: We have synthesized TiO_2, ZrO_2 nanoparticles utilizing sol-gel method and PVA, PVA/nanoparticles composite membrane prepared through solution casting technique. The as prepared nanoparticles and composites were characterized through X-ray diffraction (XRD) study, atomic force microscopy (AFM), field emission scanning electron microscopy (FESEM), X-ray photoelectron spectroscopy (XPS), Fourier transform infrared (FTIR) spectroscopy, transmission electron microscopy (TEM), UV-Vis spectroscopy and photoluminescence spectroscopy (PL) analysis to explore the structural, morphological, surface chemistry, optical properties and chemical bonds presents in the samples. The details of the experimental arrangements employed in our work have been described in the following sections.The diverse uses of polymer nanocomposites in packaging of food, coatings, air and water purification, batteries and solar cells have led to substantial research into these materials [1-4]. Among the different polymer polyvinyl alcohol (PVA) focused much attention as result of its distinctive qualities, like environment friendly, solubility in water, non-toxic, biodegradable, excellent optical and electrical properties, charge storage capability and chemical stability [5-8]. Several studies show the different applications of PVA when tuned its optical and structural properties by doping [9-13]. The OH group in PVA is responsible for majority of the physical properties that gives rise to the substances wide range of industrial uses [14]. Nanocomposites made of an organic polymer and inorganic material are gaining a much attention because of their outstanding properties and numerous uses [15-17]. The fabrication of inorganic and organic hybrid systems devices like optoelectronic devices, solar cell and photoelectrode can result in the invention of novel devices technologies [18-20]. Polymer/ceramic oxide composites have also received a lot of research attention for the separator of supercapacitors [21, 22]. Lithium-ion batteries are promising alternatives for portable gadgets and electric cars because of its small size, cheap maintenance, extended life cycle and higher energy density [23]. However, increasing the lithium-ion batteries use into novel energy storage devices with low self-discharge requires improved battery safety [24-26]. Yanilmaz et al. reported separators play a crucial role to prevent short circuits through restricting physical connection between electrodes. Simultaneously, allowing the movement of lithium-ions between them during cycles of charging and discharging. The separators must have appropriate pore size, exceptional thermal and chemical stability, sufficient thickness and superior permeability to lithium-ions. [27].

Xiao et al. reported that PVA serves a famous as a superior material for membranes because of its exceptional qualities including good film-forming ability and superior mechanical, chemical, and thermal stabilities. Numerous investigations have been conducted since the introduction of membranes based on PVA as separators in diverse fuel cells. PVA, a crucial component of the gel electrolyte in microbial fuel batteries, has generated a lot of interest [28]. Doping of inorganic ceramic oxide nanoparticles can enhance characteristics of PVA membranes. It has been discovered that doping of ceramics oxides to the polymer matrix increases ionic conductivity because they add porosity to the PVA matrix by expanding the amorphous areas

of the crystalline polymer [29]. According to studies, incorporating inorganic particles into separator membranes is a good strategy to increase thermal stability and electrochemical performance [30-33].
A lot of interest has been paid to titanium dioxide (TiO_2) because of its promising qualities. It is an inorganic semiconductor with a large band gap that finds extensive use in various fields, such as air and water purification, photocatalysis, sensors and self-cleaning windows [34]. Anatase, brookite and rutile is the three main phases of TiO_2. The utmost stable phase of TiO_2 was discovered to be rutile, while the other two (anatase and brookite) are metastable forms [35, 36]. When TiO_2 and PVA polymer are combined, they may interact in the polymers crystalline or amorphous regions, changing its electrical, structural and optical characteristics [37].
Gupta et al. reported the ball milling process for the preparation of TiO_2 nanoparticles in order to increase the photocatalytic activity and mechanical strength and suggest that by optimizing the rotating speed, ball to grinding material ratio and grinding time the desired properties of grinding material may be tuned [38]. Ramakrishnan et al. investigated solvothermal and microwave techniques to produce TiO_2 nanoparticles for use in dye-sensitized solar cells [39]. Campos et al. explored the biogenic synthesis of TiO_2 by employing the extract of Annona muricata L. as an organic reductant and stabilizing agent. TiO_2 nanoparticles efficiency in the photocatalysis process was pointed out, highlighting its potential uses in the area of photocatalysis and the destruction of organic pollutants [40].
In this paper sol gel technique were used to prepare TiO_2 nanoparticles of different phases like brookite, rutile and brookite-rutile mixed by controlling calcination temperature. The PVA/TiO_2 membrane prepared by solution casting technique were different phases of TiO2 have been dispersed in PVA matrix. TiO_2 nanoparticles and PVA/TiO2 nanocomposite membranes optical, structural and morphological characteristics were investigated using XRD, UV-visible spectroscopy, FTIR, PL spectroscopy, TEM and AFM techniques. The proposed solution casting method has a number of advantages, including low cost, controllable morphology, uniform dispersion and scalability. The selection of TiO_2 phase and its doping into PVA matrix can significantly influence the characteristics of the resulting composites and their suitability for various applications.

Experimental Techniques:

Synthesis method of TiO_2 nanoparticles:

Sol-gel technique was used to synthesize TiO_2 nanoparticles. Titanium tetraisopropoxide (TTIP), used as a precursor of TiO_2. Initially, we prepare a solution of 80 ml ethanol and 20 ml methanol, then we add 0.04M TTIP to the solution while continuously stirred using a magnetic stirrer. The pH of the solution was kept between 2 to 3 by adding HCl and continued to stirring for
next three hours. After that, the reaction is stopped by adding 50 ml distilled water and then stirring more for one to two hours. After three days of ageing at ambient temperature, the sample had been dried to 85 °C utilizing a hot plate, then grinding for 30 minutes. Finally, the prepared powder calcined for two hours at 300°C.

Synthesis method of ZrO_2 nanoparticles:

Sol-gel technique was also used for synthesize ZrO_2 nanoparticles. As a precursor of zirconia, zirconium (IV) acetate hydroxide have been used. 0.058M zirconium acetate hydroxide was added in 100 ml of distilled water then around 30 minutes, the solution was stirred. The solutions pH was adjusted using NH_4OH solution to 7-8. To enhance ageing, the solution stirred continuously overnight and the water was then removed by centrifuging. Following that, the sample rinsed by water and ethanol and then filtered through filter paper. The collected gel has been dried around 70°C and crushed for obtain a fine powder. Finally, the prepared powder calcined for two hours at 650 °C.

Preparation of pure PVA membranes:

To fabricate PVA membranes, we first prepare PVA solution by dissolving 1 gm PVA in 20 ml deionized water and stirred at 80 °C up to it became transparent. Transparent PVA film was produced by pouring this solution in a Petri dish then leaving it at room temperature to dry.

Synthesis method of PVA/TiO_2composite membranes:

Solution casting technique was utilized to produce PVA/TiO_2 composite membranes. To prepare TiO_2 solution, 0.05 grams of TiO_2 nanoparticles were mixed in distilled water of 10 ml and sonicated for 1 hour. Simultaneously, PVA solution obtained employing the method outlined in section 5.2.3. In order to produce uniform TiO_2 nanoparticles dispersion inside the PVA, the prepared TiO_2 solution was combined with the PVA solution and this mixture was then
sonicated for two hours. The resultant mixture was then put into a Petri dish and allow to two days drying at ambient temperature. After that, the dried membrane was removed and sliced into a suitable size for further investigation.

Synthesis method of PVA/TiO_2/ZrO_2 composite membranes:

Utilizing the method outlined in section 5.2.3, we first prepare the PVA solution. Simultaneously, separate solutions for ZrO_2 and TiO_2 nanoparticles were prepared. Specifically, 0.05 grams of each TiO_2 and ZrO_2 nanoparticles were dispersed individually in 10 ml of distilled water within separate beakers, employing ultrasonication for effective dispersion. Then the prepared TiO_2 and ZrO_2 solution were directly mixed with the PVA solution and sonicated for one hour to achieve homogeneous dispersion of TiO_2 and ZrO_2 nanoparticles in PVA matrix. After that, the PVA/TiO_2/ZrO_2 mixture was put to a clean Petri dish then allowed two days of drying at ambient temperature. The obtained uniform ceramic oxides dispersed PVA membrane was taken out of the Petri dish.

Result and discussion:

UV-Vis Spectroscopy:

In order to ascertain a material's bandgap, UV-Vis spectroscopy is a crucial method. Using this method, the intensity of light (I) passes by the sample is compare with the initial light intensity (I_0) prior to entering the sample. UV-Visible spectroscopy investigates the molecules' electronic transitions when they absorb light from the electromagnetic spectrum's ultraviolet and visible regions.
Optical absorbance measurements have been performed at ambient temperature utilizing the UV-visible spectrometer [950, Perkin Elmer Lambda (MANIT, Bhopal)] in the spectral range between 200 nm to 1100 nm at room temperature. The instrument records a wavelength versus absorbance graph automatically. The photograph of UV-visible spectrometer is shown in Figure 2.2.

Figure 2.2: Perkin Elmer Lambda 950 UV-visible spectrometer.

Schematic figure of double beam ultraviolet (UV)-spectrophotometer is represents in the Figure 2.3. Tungsten,

xenon arc lamp and deuterium lamps were used as light sources. A beam of specified wavelength is passed with the sample. The lamp emits infrared, visible, or ultraviolet light, entered into the monochromators, which disperse the light and select the specific wavelength that the operator has selected for the measurement.
Light of the selected wavelength hits a beam splitter which splits the light emitted from the monochromators in two beams. One beam goes through the sample, while the other beam goes through the reference. The absorbance of the sample and reference sample can be measured simultaneously. Light detector detects the wavelength that the sample has absorbed and compares it to the wavelength absorbed by reference samples. Amount of light absorbed or transmitted by the sample can be calculated by examining the intensity of the two beams strike the detector.
An absorption spectrum is generated using an automated recording system equipped with a scanning mechanism that alters the wavelength configuration of the monochromators while simultaneously operating the chart recorder.

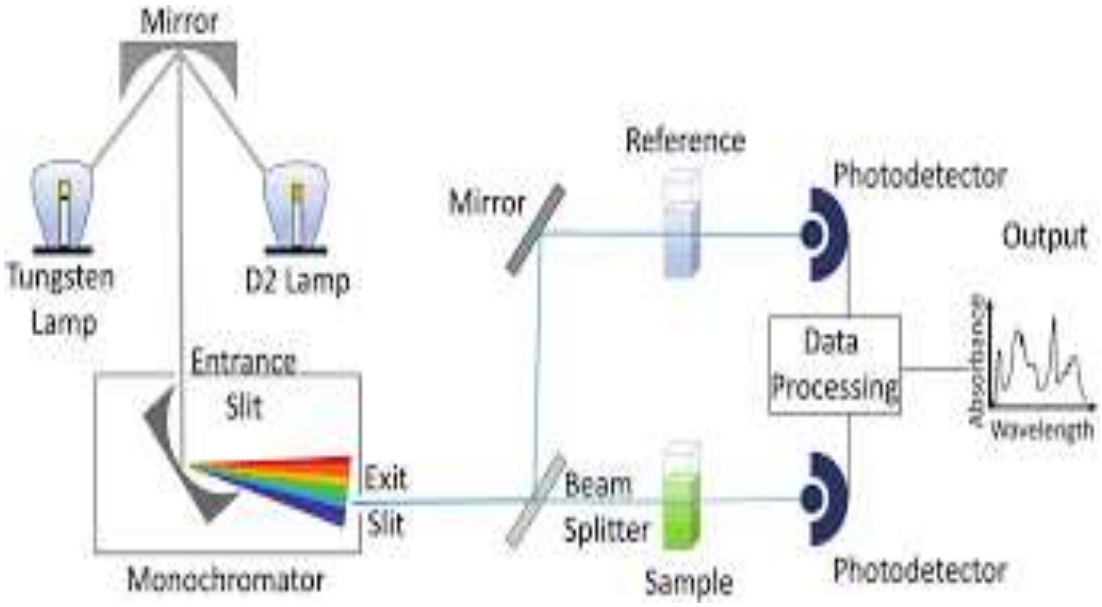

Figure 2.3: Schematic illustration of a double beam ultraviolet (UV)-spectrophotometer [2].

When the organic compounds absorb UV radiation in the visible and ultraviolet range involves the transition of electrons in σ, π, and n-orbitals via their initial ground state to a higher energy state.
These elevated energy states are characterized by molecular orbitals that are unoccupied in the ground state and are commonly referred to as anti-bonding orbitals. The anti-bonding orbital associated with a σ bond is referred to as the σ* orbital, while the anti-bonding orbital linked to a π bond is known as the π* orbital.

PL Spectroscopy:

PL spectroscopy has a convenient and non-destructive technique for investigating the materials optical properties. The approach that allows photons, or electromagnetic radiation, tends to be absorbed by material and subsequently reradiates photons is known as photoluminescence. This makes sense in terms of quantum mechanics: a photon is released to return to a state of lowered energy after being excited to a state of greater energy. It is reasonable to transferred an electron through the valence band to the conduction band, crossing the forbidden energy gap, if a photon's energy exceeds the band gap energy. An image of PL spectrometer is displays in Figure 2.4.

Figure 2.4: Hitachi F-7000 PL spectrometer.

The spectra of PL for TiO_2, ZrO_2 nanoparticles and their PVA composite membranes were recorded using Hitachi F-7000 PL spectrometer from MANIT, Bhopal. Schematic figure of PL spectrometer is shown in Figure 2.5.

The primary components of a PL spectrometer include a source of light, two monochromators, a holder for samples and a detector. A xenon flash tube is used as the excitation source, which emits intense pulse across the instrument spectral range. Two monochromators are employed: the one to determine the excitation wavelength and the second for evaluating the light that is released. With respect to the excitation beam, the detector is angled at 90-degree.

Light is directed to the excitation monochromator via the optical system, enabling either identifying of a particular wavelength within the range or wavelength pre selection. Exciting light thereafter comes into the specimen chamber that contains fluorescent cuvette. The specialized cuvette designed for fluorescence measurements is utilized, featuring four translucent sides made of either quartz or glass. When the light hits the sample cell, it excites the molecules present in the solution, and some of them will emit light. Emitted light at the right angle of the incoming beam is analyzed with the help of emissions monochromator. The examination of wavelength of the released light carried out via calculating the wavelength-specific fluorescence intensity which are preselected. Emitted light of pre-selected wavelength is goes to the detector by the analyzer monochromator. The intensity of light is measured by using a photomultiplier tube as a detector. The measuring device receives the output current from the photomultiplier, which indicates the extent of fluorescence.

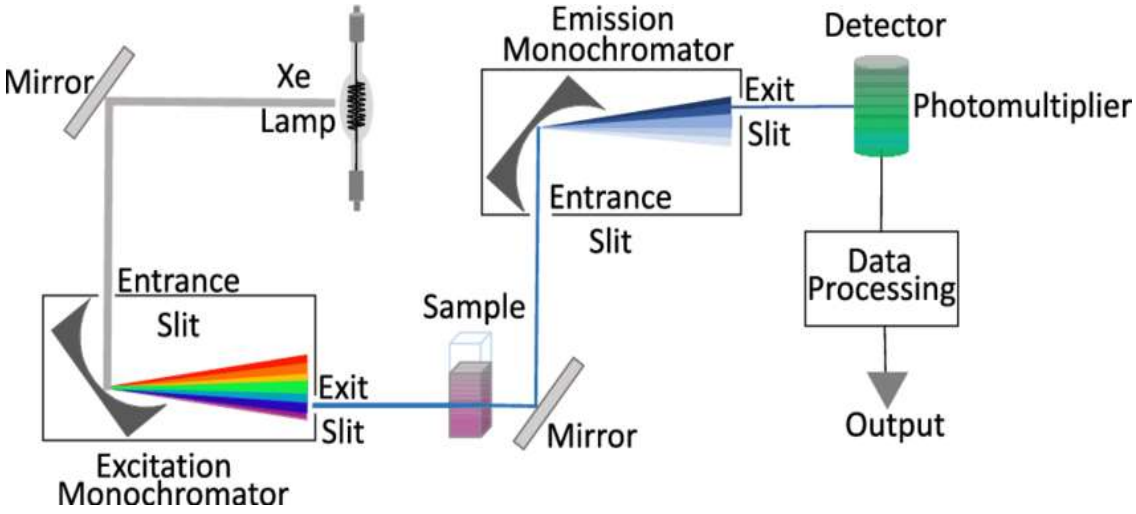

Figure 2.5: Schematic diagram of a photoluminescence (PL) spectroscopy [3].

Figure 3.2 illustrates the three distinct crystalline polymorphs of TiO_2 namely brookite anatase, and rutile**.** Each of these structures has a unique atomic arrangement and lattice symmetry. Rutile and Anatase has a tetragonal crystal structure. In the both structures, each titanium (Ti) atom is surrounded by six oxygen atoms, and each oxygen (O) atom bonded with three titanium (Ti) atoms. forming octahedral coordination. In every instance, there exists a slight distortion in the TiO_6 octahedron, where two Ti—O bonds are slightly greater than the remaining four. Furthermore, certain angles of O—Ti—O bond deviate by the expected 90 degrees. Anatase exhibits a higher distortion compared to rutile. The crystal structures of both rutile and anatase are commonly explained as chains of TiO_6 octahedra with shared edges. Specifically, rutile shares two edges while anatase shares four edges. rutile is the most stable and commonly occurring form of TiO_2 at higher temperatures. Once the formation of the rutile phase occurred, its growth rate notably surpassed that of the anatase phase.

Brookite TiO_2 has an orthorhombic crystal system. Brookite is the least common phase among the three major TiO_2 crystal structures. It is typically found in lower-temperature and high-pressure conditions. The composition of its unit cell consists of eight TiO_2 formula units, which forms through the TiO_6 octahedra that share edge. It possesses greater complexity, exhibits a greater cell volume and being less dense in comparison with two other phases.

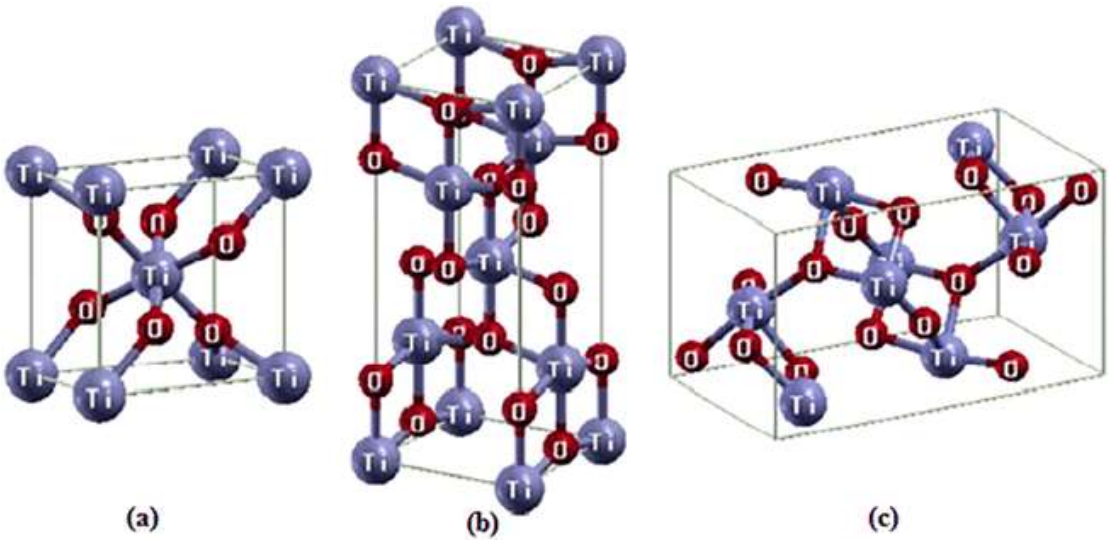

Figure 3.2: TiO_2 crystal structures consisting of (a) anatase, (b) rutile, and (c) brookite [41].

UV Absorption Spectroscopy:

Figure 3.3 illustrates absorption spectra of PVA and PVA/TiO_2 nanocomposite membranes containing various TiO_2 phases. The pure PVA membrane absorption spectrum exhibits two absorption band at 275 and 332 nm, correspond to the electronic transitions $\pi \rightarrow \pi^*$ and $n \rightarrow \pi^*$ respectively [46, 47].

In PVA/TiO_2 nanocomposite membranes containing various TiO_2 phases [Figure 3.5 (b), 3.5 (c), 3.5 (d)], the band correspond to $\pi \rightarrow \pi^*$ transitions have been shifted from 275 nm to 277 nm, 281 nm and 290 nm for PVA/TiO_2 (brookite), PVA/TiO_2 (brookite-rutile) and PVA/TiO_2 (rutile) composite respectively. Additionally, the second identified band due to $n \rightarrow \pi^*$ electronic transitions shifted from 332 nm to 334 nm, 343 nm and 357 nm for the same respective composites. As can be observed in the figure, a new band was discovered in all PVA/TiO_2 nanocomposite membranes. This band corresponds to TiO_2 nanoparticles at positions 371 nm for PVA/TiO_2 (brookite), 372 nm for PVA/TiO_2 (brookite-rutile) and 377 nm for PVA/TiO_2 (rutile). The new band appearance, indicates the formation of complex (which is causes by a hydrogen bonding among the Ti ions and adjoining OH group of PVA) [34].

Further we also observed that all prepared nanocomposite membranes showed a remarkable increase in absorbance intensity, which is caused by the strong interaction between PVA and TiO_2. Therefore, the shifting of the bands towards the region of higher wavelength (known as red shift) coinciding with the intensity increases, indicates that the utilization of nanofillers in small quantities could be tuned the PVA band gap [48].

Based on the comparison of doping effects of various phase reveals that absorption edge of the PVA/TiO_2 (rutile) nanocomposite membrane is shifts greater compare to other two phases. We also observed that the enhancement in absorption intensity is greater for PVA/TiO_2 (brookite-rutile) nanocomposite. Since PVA/TiO_2 nanocomposite films showed selective absorption in the UV range. Therefore, due to ability to selective absorption, rendering them useful as ultraviolet filters.

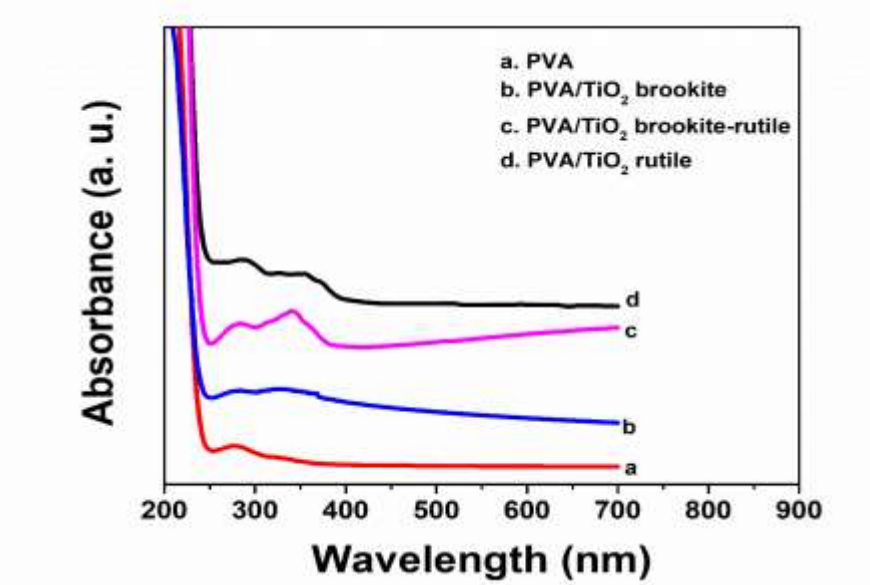

Figure 3.3: Absorption spectra of (a) PVA membrane, (b) PVA/TiO2 brookite, (c) PVA/TiO2 brookite-rutile TiO2, (d)PVA/TiO2 rutile membrane.

Photoluminescence Study:

The PVA and PVA/TiO2 nanocomposite membranes photoluminescence spectra obtained at a 300 nm excitation wavelength have been illustrated in Figure 3.4.

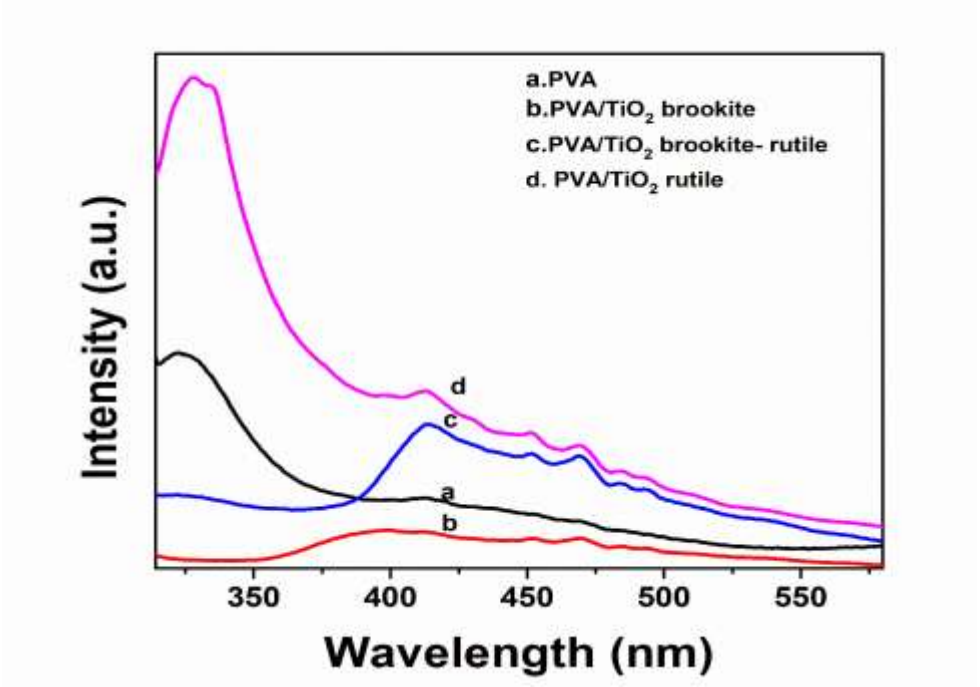

Figure 3.4: PL spectra for PVA and PVA/TiO2 composite membranes using excitation wavelength 300 nm (a) PVA, (b) PVA/TiO2 (brookite), (c) PVA/TiO2 (brookite-rutile), (d) PVA/TiO2 (rutile).

The membrane of pure PVA [Figure 3.9 (a)], exhibits a broad emission band is a result of the hydroxyl groups electronic transitions π*→n, which signify the presence of atactic, isotactic and syndiotactic polymer configurations to the aqueous solution [68]. Figure 3.9 (b), (c) and (d) illustrates the PL spectra obtained from PVA/TiO2 (brookite), PVA/TiO2 (brookite-rutile) and PVA/TiO2 (rutile) membranes. One intense emission peak has been observed at 329 nm, while six more emission bands can be seen at approximately 397 nm, 412 nm,
451 nm, 469 nm, 484 nm and 494 nm in the PL spectra of PVA/ TiO2 (rutile) composite membrane. The intense emission peak at 329 nm have been contributed from the emission of TiO2 nanoparticles [band to band transitions]. The reason for this peak in high intensity is the transfer of electrons from TiO2 rutile nanoparticles to PVA via the heterogeneous interface between the two conduction bands, because TiO2 rutile phase has a direct bandgap. The detected emission band at 397 nm signifies the band gap recombination of TiO2 [69]. Peak at 412 nm is associated with the band transition of TiO2 [70].
The PL bands observed at 451 and 469 nm corresponds to the band edge free excitons [71, 72]. The other two peaks, which occur at 484 and 494 nm have been determined to be bound exciton. In the case of PVA/TiO2 (brookite) and PVA/TiO2 (brookite-rutile) composite membranes, the intense emission peak has disappeared and the intensity of other peaks has decreased. Furthermore, we observed that the PL peak intensity of the PVA/TiO2 (brookite) composite membrane is significantly lower than that of the other two composite membranes. The PL emission is directly related to recombination of holes and excited electrons, so it could be predicted that higher intensity of PL emission indicates faster recombination of charge carrier which is not favorable for high photocatalytic activity. While, lower intensity of PL emission indicates the utmost charge carrier's separation, that is highly beneficial for effective photocatalytic performance [73, 74]. TiO2 (brookite) doping into PVA matrix show less PL peak intensity similar results also observed by Dey et al. indicating that doping is useful for preventing photogenerated charges from recombination [75]. Doping produces oxygen vacancies and crystal defects that trap photoinduced charges [76]. The results of the doping of PVA with three distinct phases of TiO2 show that PVA/TiO2 (brookite) membrane has better photocatalytic activity than PVA/TiO2 (brookite-rutile) and PVA/TiO2 (rutile) membranes [77]. High photocatalytic activity of composite membrane is advantageous for lithium-ion battery applications, since it

lowers impurities and enhances overall battery performance.

UV-Visible Study:

The absorption spectra of PVA and PVA/ZrO_2 composite membranes are shown in Figure 4.3. For pure PVA membrane two absorption peaks observed at 275 nm and 332 nm. These peaks are corresponded to the π→π* and n→π* electronic transitions respectively [23, 24]. Doping of ZrO_2 nanoparticles with different concentrations in the PVA matrix as shown in figure, the band correspond to π→π* transitions were shifted from 275 nm to 277 nm, 279 nm and 284 nm for PVA/ZrO_2 (5 wt%), PVA/ZrO_2 (9 wt%) and PVA/ZrO_2 (13 wt%) respectively. While the second observed band due to n→π* electronic transitions of PVA is diminished in composite structure. For the absorption spectra of PVA/ZrO_2 (5 wt%) membrane shown in Figure 4.3 (b) the new band observed at 360 nm which
corresponds to ZrO_2 nanoparticles. A systematic red shift was also observed in the position of the band corresponds to ZrO_2 centered from 360 nm to 363nm and 364 nm for PVA/ZrO_2 (9 wt%) and PVA/ZrO_2 (13 wt%) respectively. The observed red shift in the absorption peak positions of PVA/ZrO_2 composites with increasing the weight percent of ZrO_2 in the PVA matrix indicates that small amounts of nanofiller could be used to change the optical band gap of PVA [25]. The results further confirmed that ZrO_2 nanoparticles interact strongly with PVA. Further we also observed that with increasing the ZrO_2 concentration in PVA, all prepared nanocomposite membrane showed a remarkable increase in absorbance indicating its potential applications in filters and UV-shielding. This was attributed to the free electrons of the nanoparticles absorbing excess light radiation [26].

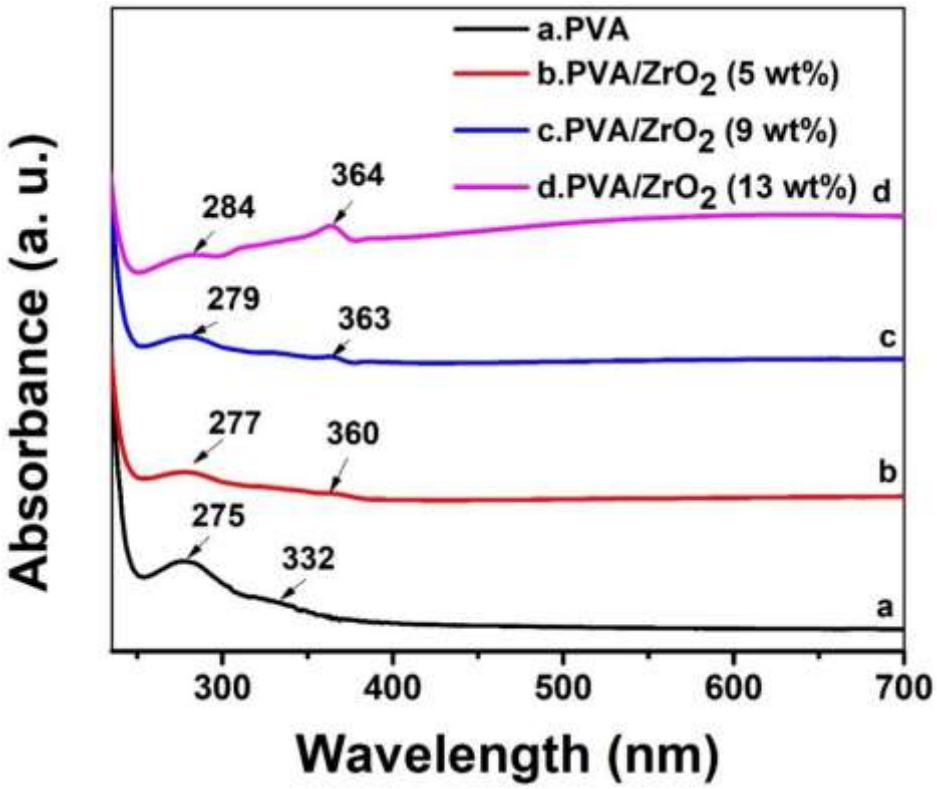

Figure 3.5: Absorption spectra of PVA and PVA/ZrO_2 composite membranes (a) PVA, (b) PVA/ZrO_2 (5 wt%), (c) PVA/ZrO_2 (9 wt%), (d) PVA/ZrO_2 (13 wt%).

Photoluminescence:

The photoluminescence spectra of ZrO_2 nanoparticles using excitation wavelength of 300 nm shown in Figure 4.4. The spectra exhibit four bands at 397, 448, 465 and 530, nm. The 397 nm emission band is attributed to the near band edge emission (NBE), the present case confirms high ZrO_2 crystallinity [27, 28]. The peaks at 448 and 465 nm are caused by mid-gap trap states, such as defects on surface and oxygen vacancies [29-31]. The peak around 530 nm can be noticed which might be assigned to the presence of interstitial Zr^{3+} ions as defects [32, 33].

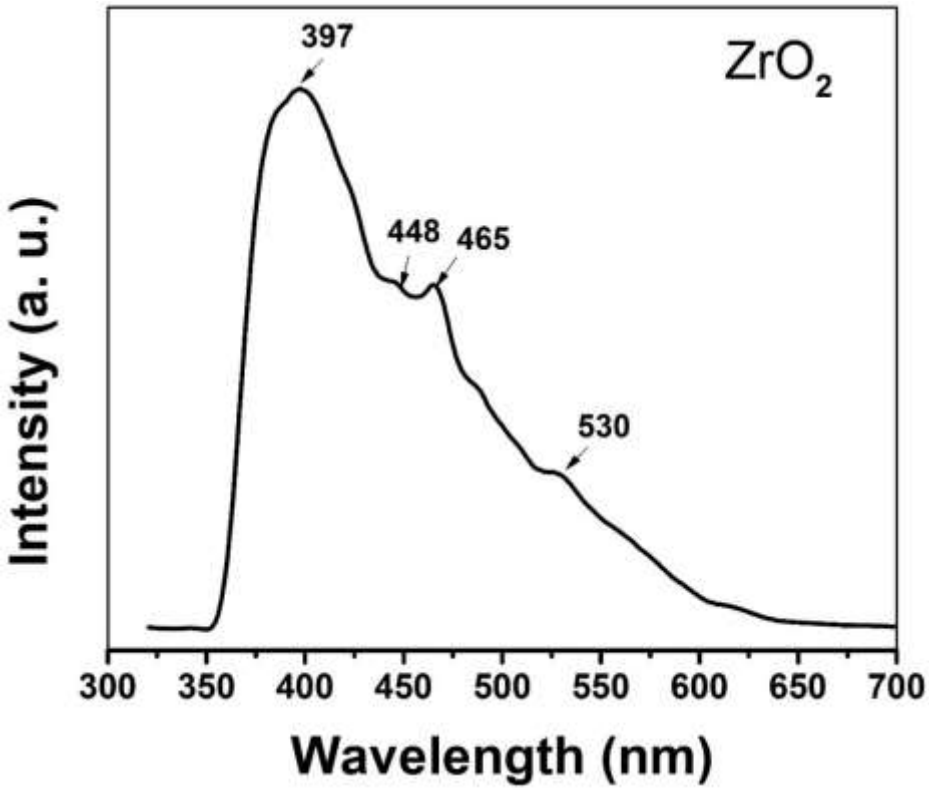

Figure 4.4: PL spectra of ZrO_2 nanoparticles using excitation wavelength 300 nm.

The Photoluminescence spectra of PVA and PVA/ZrO_2 composite membranes with different concentration of ZrO_2 shown in Figure 4.5. The broad emission bands observed in pure PVA membrane correspond to $\pi^* \rightarrow n$ electronic transitions of OH groups, which is the characteristic of three different aqueous solution polymer configurations: isotactic, syndiotactic, and atactic [34]. The PL spectra of PVA/ZrO_2 [5 wt%, 9 wt% and 13 wt%] composite membrane shows luminescence peaks corresponding to the ZrO_2 nanoparticles were observed in all composite membrane. Variations in emission intensity are related to the filler concentration and is observed to be maximum for 5 wt% concentration of ZrO_2 in PVA/ZrO_2 membrane. As the concentration of filler increases the photoluminescence intensity of PVA/ZrO_2 composite membranes decreased. At higher concentration the decreases in PL intensity of composite membranes may be due to the self - absorption of light [1]. Photoluminescent property of PVA/ZrO_2 composite membrane shows its potential application in diode.

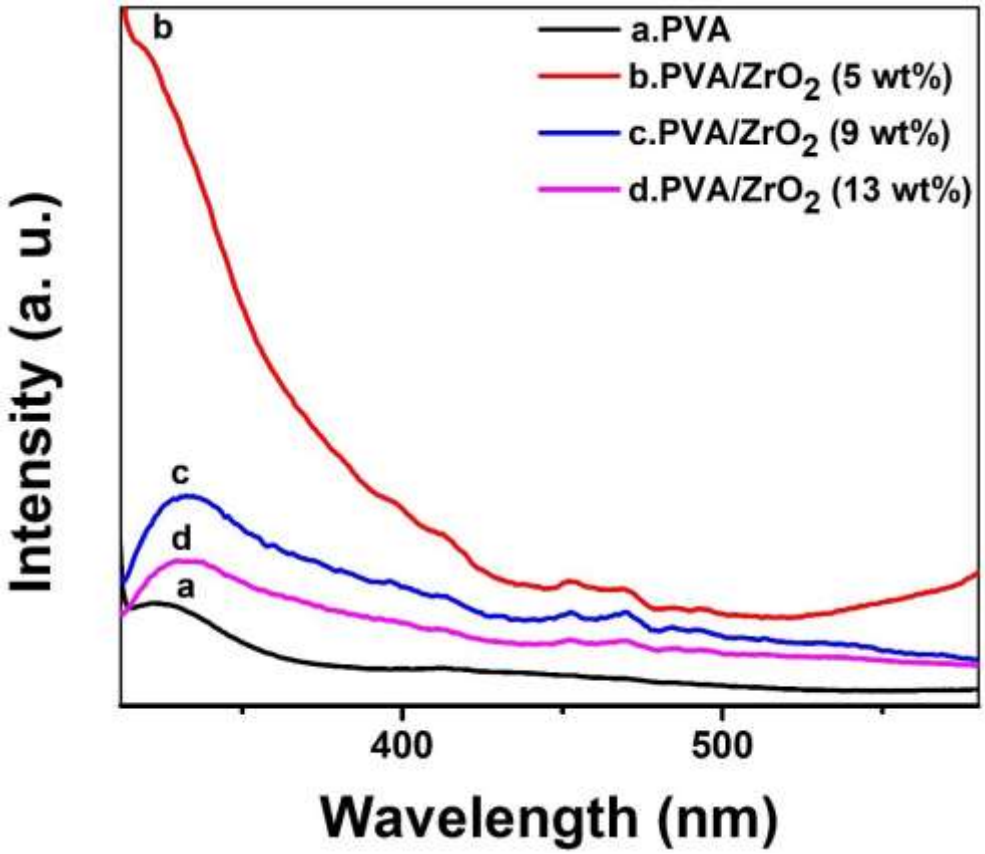

Figure 4.5: PL spectra for PVA and PVA/ZrO_2 composite membranes using excitation wavelength 300 nm (a) PVA, (b) PVA/ZrO_2 (5 wt%), (c)) PVA/ZrO_2 (9 wt%), (d)) PVA/ZrO_2 (13 wt%).

References:

1. A. Kausar, J. Plast. Film Sheet. 2019, 36, 94-112.

2. A. Mills, S. Le Hunte, J. Photochem. Photobiol. A, 1997, 108, 1-35.

3. Y. Paz, Appl. Catal. B: Environ. 2010, 99, 448-460.

4. A. N. Abougreen, A. E. Shalan, E. S. A. Serea, M. K. A. Mohammed, in Advances in Nanocomposite Materials for Environmental and Energy Harvesting Applications, Springer International Publishing, Switzerland, 2022, pp. 697-724.

5. R. Kochi, V. Crasta, N. B. Rithin Kumar, G. Shetty, P. D. Rekha, J. Polym. Res. 2019, 99, 1.

6. N. B. Halima, RSC Adv. 2016, 6, 5774-5796.

7. J. O. Dennis, M. F. Shukur, O. A. Aldaghri, K. H. Ibnaouf, A. A. Adam, F. Usman, Y. M. Hassan, A. Alsadig, W. L. Danbature, B. A. Abdulkadir, Molecules, 2023, 28, 1781.

8. X. Jiang, C. Y. Wang, Q. Han, Comput. Theor. Chem. 2017, 1102, 15-21.

9. M. Aslam, M. A. Kalyar, Z. A. Raza, J. Electron. Mater. 2019, 48, 1116–1121.

10. S. I. Ahn, K. Kim, J. R. Jung, K. Y. Kang, S. M. Lee, J. Y. Han, K. C. Choi,

Chem. Phys. Lett. 2015, 625, 36.

11. K. J. Ramalingam, N. R. Dhineshbabu, S. R. Srither, B. Saravanakumar, R. Yuvakkumar, V. Rajendran, Synth. Met. 2014, 191, 113.
12. S. B. Aziz, J. Electron. Mater. 2016, 45, 736.

13. T. A. Hamdalla, T. A. Hanafy, A. E. Bekheet, J. Spectrosc. 2015, 1.

14. R. K. Tubbs, J. Polym. Sci., Part A-1: Polym. Chem. 1966, 4, 623–629.
15. V. R. Mehto, A. Mehto, D. K. Gupta, R. K. Pandey, J. Chin. Chem. Soc. 2016, 63, 935–946.
16. D. C. Schnitzler, A. Zarbin, J. Braz. Chem. Soc. 2004, 15, 378-384.

17. P. Judeinstein, C. Sanchez, J. Mater. Chem. 1996, 6, 511-525.

18. S. J. Devaki, R. Ramakrishnan, in Advances in Nanostructured Composites, CRC Press, United Kingdom, 2019, pp. 352-375.
19. L. E. Greene, M. Law, B. D. Yuhas, P. D. Yang, J. Phys. Chem. C, 2007, 111, 18451-18456.
20. J. Zhou, H. Cheng, J. Cheng, L. Wang, H. Xu, Small Methods, 2024, 8, 2300418.
21. S. Ahankari, D. Lasrado, R. Subramaniam, Mater. Adv. 2022, 3, 1472-1496.

22. C. O. Alvarez-Sanchez, J. A. Lasalde-Ramírez, E. O. Ortiz-Quiles, R. Massó-Ferret, E. Nicolau, Energy Sci. Eng. 2019, 7, 730-740.
23. M. H. Hossain, M. A. Chowdhury, N. Hossain, M. A. Islam, M. H. Mobarak, Chem. Eng. J. Adv. 2023, 16, 100569.
24. H. Jeon, D. Yeon, T. Lee, J. Park, M. H. Ryou, Y. M. Lee, J. Power Sources, 2016, 315, 161–168.
25. Y. Wang, S. Wang, J. Fang, L. X. Ding, H. Wang, J. Membr. Sci. 2017, 537, 248–254.
26. S. Ye, D. Zhang, H. Liu, J. Zhou, J. Appl. Polym. Sci. 2011, 121, 1757–1764.

27. M. Yanilmaz, J. Text. Inst. 2019, 111, 1–6.

28. W. Xiao, L. Zhao, Y. Gong, J. Liu, C. Yan, J. Membr. Sci. 2015, 487, 221–228.
29. C. Y. Bon, L. Mohammed, S. Kim, Manasi, P. Isheunesu, K. S. Lee, J. M. Ko, J. Ind. Eng. Chem. 2018, 68, 173.
30. Y. C. Nho, J. Y. Sohn, J. Shin, J. S. Park, Y. M. Lim, P. H. Kang, Radiat. Phys. Chem. 2017, 132, 65–70.
31. D. Wu, L. Deng, Y. Sun, K. S. Teh, C. Shi, Q. Tan, J. Zhao, D. Sun, L. Lin, RSC Adv. 2017, 7, 24410–24416.
32. J. Cao, L. Wang, Y. Shang, M. Fang, L. Deng, J. Gao, J. Li, H. Chen, X. He, Electrochimica Acta, 2013, 111, 674–679.
33. S. Zhang, J. Cao, Y. Shang, L. Wang, X. He, J. Li, P. Zhao, Y. Wang, J. Mater. Chem. A, 2015, 3, 17697–17703.
34. S. D. Praveena, V. Ravindrachary, R. F. Bhajantri, Ismayil, Polym. Compos. 2014, 37, 987–997.
35. W. W. So, S. B. Park, K. J. Kim, C. H. Shin, S. J. Moon, J. Mater. Sci. 2001, 36, 4299–4305.

36. S. Bakardjieva, V. Stengl, L. Szatmary, J. Subrt, J. Lukac, N. Murafa, D. Niznansky, K. Cizek, J. Jirkovsky, N. Petrova, J. Mater. Chem. 2006, 16, 1709–1716.
37. Y. Khairy, H. I. Elsaeedy, M. I. Mohammed, H. Y. Zahran, I. S. Yahia, Polym. Bull. 2019, 77, 6255–6269.

38. A. Gupta, K. Kushwah, S. Mahobia, P. Soni, V. V. Murty, Int. J. Innov. Technol. Explor. 2019, 8, 2462-2465.
39. V. M. Ramakrishnan, S. Pitchaiya, N. Muthukumarasamy, K. Kvamme, G. Rajesh, S. Agilan, D. Velauthapillai, Int. J. Hydrogen Energy, 2020, 45, 27036-27046.
40. D. Asmat-Campos, M. L. Rojas, A. Carreño-Ortega, Clean. Eng. Technol. 2023, 17, 100702.
41. M. Kaur, K. Singh, Mater. Sci. Eng. C, 2019, 102, 844-862.

42. I. Morad, X. Liu, J. Qiu, J. Am. Ceram. Soc. 2020, 103, 3051–3059.
43. B. Pejova, I. Grozdanov, Mater. Chem. Phys. 2005, 90, 35–46.

44. M. Abdelaziz, M. M. Ghannam, Phys. B: Condens. Matter, 2010, 405, 958-964.

45. M. Abdelaziz, Phys. B: Condens. Matter, 2011, 406, 1300–1307.

46. A. M. Shehap, Egypt. J. Sol. 2008, 31, 75–91.

47. O. G. Abdullah, S. B. Aziz, M. Rasheed, Results Phys. 2016, 6, 1103–1108.

48. A. N. Ananth, S. Umapathy, J. Sophia, T. Mathavan, D. Mangalaraj, Appl. Nanosci. 2011, 1, 87–96.
49. A. M. Shehap, D. S. Akil, Int. J. Nanoelectron. Mater. 2016, 9, 17–36.

50. M. El-Gohary, J. Cult. Herit. 2009, 10, 471–479.

51. Z. Cai, R. Remadevi, M. A. A. Faruque, M. Setty, L. Fan, A. N. M. A. Haque, M. Naebe, RSC Adv. 2019, 9, 34076–34085.

52. Z. Corzo-González, M. I. Loria-Bastarrachea, E. Hernández-Nuñez, M. Aguilar-Vega, M. O. González-Díaz, Polym. Bull. 2017, 74, 2741–2754.
53. G. M. Kim, In Nanofibers, IntechOpen, London, UK, 2010.

54. J. Lee, J. Hong, D. W. Park, S. E. Shim, Opt. Mater. 2010, 32, 530–534.

55. G. M. Kim, A. S. Ashraf, G. H. Michler, P. Simon, J. S. Kim, Bioinspir. Biomim. 2008, 3, 046003.
56. I. Omkaram, R. P. S. Chakradhar, J. L. Rao, Phys. B: Condens. Matter, 2007, 388, 318–325.
57. E. Al-Emam, H. Soenen, J. Caen, K. Janssens, Herit. Sci. 2020, 8, 106.

58. N. Ahmed, E. M. Ahmed, J. Mater. Sci.: Mater. Electron. 2020, 31, 6139–6153.
59. A. L. Waly, A. M. Abdelghany, A. E. Tarabiah, J. Mater. Res. Technol. 2021, 14, 2962–2969.
60. R. N. Oliveira, R. Rouzé, B. Quilty, G. G. Alves, G. D. A. Soares, R. M. S. M. Thiré, G. B. McGuinness, Interface Focus, 2014, 4, 20130049.

61. N. Ahad, E. Saion, E. Gharibshahi, J. Nanomater. 2012, 2012, Article ID 637429.
62. M. Jiaojiao, L. Ying, Y. Xiande, X. Yu, Y. Jia, B. Jianjun, Z. Tao, RSC Adv. 2016, 6, 49448–49458.
63. U. Siemann, in Scattering Methods and the Properties of Polymer Materials, Springer, Berlin/Heidelberg, Germany, 2005, pp. 1–14.
64. A. Tawansi, A. H. Oraby, H. M. Zidan, M. E. Dorgham, Phys. B: Condens. Matter. 1998, 254, 126–133.

65. P. B. Bhargav, V. M. Mohan, A. K. Sharma, V. V. R. N. Rao, Ionics, 2007, 13, 441–447.
66. W. Yuping, X. Zongli, N. G. Derrick, S. Shirlene, Z. Zhonghua, J. Appl. Polym. Sci. 2017, 134, 44839.
67. R. P. Pandey, V. K. Shahi, J. Membr. Sci. 2013, 444, 116–126.

68. D. M. Fernandes, A. A. Winkler Hechenleitner, S. M. Lima, L. H. C. Andrade, A. R. L. Caires, E. A. Gómez Pineda, Mater. Chem. Phys. 2011, 128, 371–376.
69. X. F. Lei, X. X. Xue, H. Yang, Appl. Surf. Sci. 2014, 321, 396–403.

70. S. Jia, X. Li, B. Zhang, J. Yang, S. Zhang, S. Li, Z. Zhang, Appl. Surf. Sci. 2019, 463, 829–837.
71. Q. J. Xiang, K. L. Lv, J. G. Yu, Appl. Catal. B: Environ. 2010, 96, 557–564.